Toward surface quantification of liver fibrosis progression

Yuting He
Singapore-MIT Alliance
E4-04-10
4 Engineering Drive 3
Singapore 117576
and
A*STAR
Institute of Bioengineering and Nanotechnology
Singapore 138669

Chiang Huen Kang
A*STAR
Institute of Bioengineering and Nanotechnology
Singapore 138669

Shuoyu Xu
Singapore-MIT Alliance
E4-04-10
4 Engineering Drive 3
Singapore 117576
and
A*STAR
Institute of Bioengineering and Nanotechnology
Singapore 138669
and
Nanyang Technological University
School of Computer Engineering
Singapore 639798

Xiaoye Tuo
Singapore-MIT Alliance
E4-04-10
4 Engineering Drive 3
Singapore 117576
and
A*STAR
Institute of Bioengineering and Nanotechnology
Singapore 138669
and
Peoples Liberation Army General Hospital
Affiliated Hospital 1
Department Burns & Plastic Surgery
Beijing 100037, China

Scott Trasti
National University of Singapore
Comparative Medicine
Singapore 117456

Dean C. S. Tai
A*STAR
Institute of Bioengineering and Nanotechnology
Singapore 138669

Anju Mythreyi Raja
A*STAR
Institute of Bioengineering and Nanotechnology
Singapore 138669
and
National University of Singapore
Graduate School for Integrative Science and Engineering
Singapore 117456

Qiwen Peng
Singapore-MIT Alliance
E4-04-10
4 Engineering Drive 3
Singapore 117576
and
A*STAR
Institute of Bioengineering and Nanotechnology
Singapore 138669

Peter T. C. So
Singapore-MIT Alliance
E4-04-10
4 Engineering Drive 3
Singapore 117576
and
Massachusetts Institute of Technology
Department of Mechanical Engineering
77 Massachusetts Avenue
Cambridge, Massachusetts 02139

Jagath C. Rajapakse
Singapore-MIT Alliance
E4-04-10
4 Engineering Drive 3
Singapore 117576
and
Nanyang Technological University
School of Computer Engineering
Singapore 639798
and
Massachusetts Institute of Technology
Division of Biological Engineering
77 Massachusetts Avenue
Cambridge, Massachusetts 02139

Roy Welsch
Singapore-MIT Alliance
E4-04-10
4 Engineering Drive 3
Singapore 117576
and
Massachusetts Institute of Technology
Sloan School of Management
77 Massachusetts Avenue
Cambridge, Massachusetts 02139

1083-3668/2010/15(5)/056007/11/$25.00 © 2010 SPIE

Hanry Yu
Singapore-MIT Alliance
E4-04-10
4 Engineering Drive 3
Singapore 117576
and
A*STAR
Institute of Bioengineering and Nanotechnology
Singapore 138669
and
National University of Singapore
Graduate School for Integrative Science and Engineering
Singapore 117456
and
National University of Singapore
Department of Physiology
2 Medical Drive
Singapore 117597
and
National University of Singapore
Mechanobiology Institute, T-Labs
5A Engineering Drive 1
Singapore 117411

Abstract. Monitoring liver fibrosis progression by liver biopsy is important for certain treatment decisions, but repeated biopsy is invasive. We envision redefinition or elimination of liver biopsy with surface scanning of the liver with minimally invasive optical methods. This would be possible only if the information contained on or near liver surfaces accurately reflects the liver fibrosis progression in the liver interior. In our study, we acquired the second-harmonic generation and two-photon excitation fluorescence microscopy images of liver tissues from bile duct-ligated rat model of liver fibrosis. We extracted morphology-based features, such as total collagen, collagen in bile duct areas, bile duct proliferation, and areas occupied by remnant hepatocytes, and defined the capsule and subcapsular regions on the liver surface based on image analysis of features. We discovered a strong correlation between the liver fibrosis progression on the anterior surface and interior in both liver lobes, where biopsy is typically obtained. The posterior surface exhibits less correlation with the rest of the liver. Therefore, scanning the anterior liver surface would obtain similar information to that obtained from biopsy for monitoring liver fibrosis progression.
[DOI: 10.1117/1.3490414]

Keywords: liver fibrosis; second-harmonic generation; bioimaging; diagnosis; two-photon; medical optics.

Paper 10238R received May 4, 2010; revised manuscript received Aug. 3, 2010; accepted for publication Aug. 9, 2010; published online Sep. 24, 2010.

1 Introduction

Liver fibrosis is a wound-healing process in response to various toxic injuries and associated with almost all chronic liver diseases.[1–3] Inflammatory responses and excessive deposition of extracellular matrix (ECM) are often observed with cirrhosis, marking the end stage of fibrosis that is the major causes of morbidity and mortality worldwide. There is increasing evidence that fibrosis is treatable and reversible in its early stages,[4–7] and even cirrhosis can regress in some clinical studies.[8] Therefore, accurate staging of liver fibrosis is of paramount importance to determine the state of disease progression, responses to therapy, and optimization of treatment to direct disease management.[9]

Currently, researchers have reported many noninvasive methods to assess liver fibrosis. Putative serum makers of fibrosis have been evaluated for the assessment with indirect markers, including serum aminotransferase levels,[10,11] presence of coagulopathy and platelet counts[12–14] that reflect alterations in hepatic functions, and markers including laminin,[15] cytokines,[16] collagens,[17] matrix metalloproteinase, and tissue inhibitors of metalloproteinases[18,19] that reflect serum ECM deposition and turnover. Although some serum assays have been developed to diagnose significant fibrosis and cirrhosis with accuracies,[20–22] none of them has been validated as a surrogate marker to stage fibrosis due to low sensitivity or nonspecificity.[23] Radiological imaging and novel imaging modalities such as ultrasonography,[24] transient elastography,[25] and magnetic resonance elastography[26,27] which are based on liver stiffness measurements (LSM), have been shown to be reliable tools to assess liver fibrosis with quick and good reproducibility, but the sensitivity is also less satisfactory with current studies.

Percutaneous liver biopsy still represents the gold standard for the diagnosis and assessment of liver fibrosis. However, the potential complications following liver biopsy and inherent drawbacks, such as the invasive nature of the procedure, sampling error, and inter- and intraobserver variability in the interpretation of the needle biopsy results, have discouraged routine practice.[28–32] In addition, it is impractical to perform serial liver biopsies to accurately determine the changes of disease progression or to monitor the treatment effects.

To specifically and accurately monitor liver fibrosis in a quantitative manner, information extracted has to be directly compared to morphological features recognized by histological examination of liver biopsy samples. Imaging on the liver surface, especially over a larger sampling area than from biopsy, would therefore give us the potential to extract enough information over a long period of time without the complication brought forth by the invasive biopsy. Laparoscopy has been attempted to diagnose cirrhosis by surface scanning to detect the presence of nodules and the hardening of the tissue.[33,34] However, with the thick layer of capsule around the liver organ, traditional imaging technology can only focus on the capsule layer without penetrating into the tissue, making it difficult for laparoscopy to extract quantitative information based on histological information that is comparable to biopsy samples.

In recent years, second-harmonic generation (SHG) microscopy has been increasingly used to measure structural protein such as neuron, muscle, and collagen in biological samples with special structural properties.[35–40] As a nonlinear optical process, SHG exhibits intrinsic advantages over conventional fluorescence by requiring no fluorophore presence in tissue; therefore, signals are not affected by dye concentration and photobleaching. Deeper tissue penetration can also be achieved by using an infrared-range excitation source, resulting in less scattering in tissues than that in the visible wavelength range.[41–45] SHG has been applied for assessing

Address all Correspondence to: Hanry Yu, Singapore-MIT Alliance, E4-04-10, 4 Engineering Drive, Singapore 117576. Tel: 65 68247103; Fax: 65 62761755; E-mail: hanry_yu@nuhs.edu.sg

fibrosis by quantitative measurement of collagen in various organs,[36,46,47] including livers.[48–51] The results obtained using SHG/two-photon-excited fluorescence (TPEF) are standardized, highly reproducible and can monitor the progression and distribution of collagen at all stages of liver fibrosis with agreement with pathological readings.[48,51]

To incorporate such properties of SHG and TPEF imaging modalities for potential liver surface scanning based on fiber-optic endoscope[52,53] and to overcome the current drawbacks from laparoscopy, it is important to assess whether the SHG/TPEF-based methods can extract surface information that reflects the whole organ, especially the interior where biopsy samples are usually obtained. The surface distribution of liver fibrosis features also needs to be examined to direct future scanning locations on the liver surface. Therefore, fully automated quantification algorithms were developed in this paper to extract morphology-based features from both the liver surface and interior of the organ. Analysis of these features was performed to compare to the gold standard (histopathological scorings) to validate features and then to study the representativeness of surface area to the liver interior. We observed that liver anterior surfaces on both left and right lobes contain similar information as in the liver interior when imaged and extracted using SHG/TPEF imaging modalities for fibrosis analysis. This establishes the foundation for future development of laparoscopic nonlinear optical methods to serially quantify liver fibrosis on liver surfaces to eventually eliminate the need for invasive liver biopsy.

2 Methods

2.1 *Animal and Tissue Sample Preparation*

Male Wistar rats at an average weight of 220 g were housed two per cage in the Biological Resource Centre of Biopolis A*STAR with free access to laboratory chow and water in a 12:12-h light/dark schedule. All animal-related experiments were approved by the Institutional Animal Care and Use Committee. Twenty rats were randomly separated into four groups, with five control rats.

Bile duct ligation (BDL) of rats was performed under general anesthesia with ketamine (100 mg/kg body weight). A midline abdominal transverse incision was performed after shaving of the abdomen, exposing the liver and intestines. After gently displacing the liver and intestines, the lower end of the bile duct is identified at its insertion into the small intestines and traced up toward the porta, which is then doubly ligated in two areas near the porta with silk sutures (silk 3.0) and transacted between the two ligation points. Abdominal contents were gently rearranged, and the wound was closed with double-layered tissue closure with vicryl sutures. A total of 15 rats were ligated and sacrificed at intervals of 2, 4, and 6 weeks ($n=5$ per week). Five control rats were also sacrificed at week 0.

Cardiac perfusion with 4% paraformaldehyde was performed to flush out blood cells and fix the liver tissue before harvesting. Liver specimens from both the left lateral lobes and right anterior lobes were preserved in paraffin and sectioned with a thickness of 50 μm.

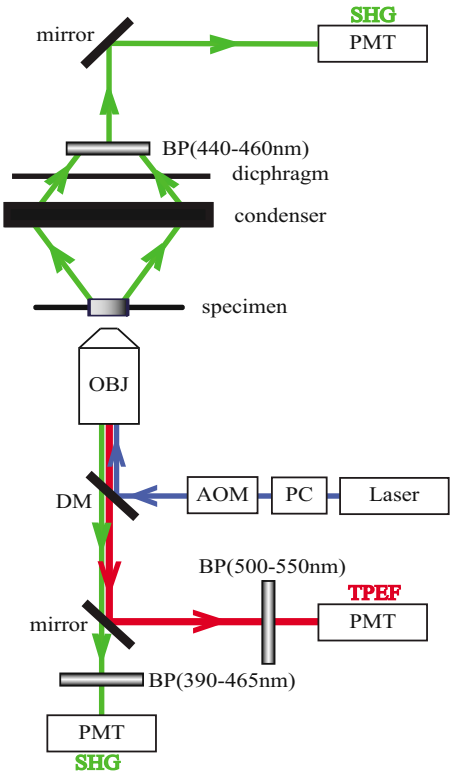

Fig. 1 Schematic illustration of the optical configuration. Excitation laser was a tunable mode-locked laser (710–990-nm set at 900 nm) with a PC and an AOM for power control. The laser went through a dichroic mirror, an objective lens (20X, NA=0.5), and reached tissue specimen. Second harmonic generation (SHG) signal was collected at the opposite side the laser source, in the transmitted mode, by a condenser (NA=0.55), through a field diaphragm, and a 440–460 nm BP filter, before being recorded by a PMT. TPEF was collected by the objective lens, filtered by a 500–550-nm BP filter, before being recorded by another PMT. Reflective SHG signal was collected on the same side as TPEF, through the 390–465-nm BP filter and recorded by PMT.

2.2 *Histopathological Scoring*

Tissue samples were stained with a Masson Trichrome (MT) stain kit (ChromaView advanced testing, no. 87019, Richard-Allan Scientific, Thermo Fisher Scientific, Wathan, Massachusetts) and whole tissue slices were imaged (Aperio Digital Pathology Environment, Aperio Technologies Inc. Vista, CA 92081). Animal tissue scoring based on whole slice MT images was performed by a pathologist based on blind reading to reduce any bias using the modified Ruwart score according to Ruwart et al.[54] and Boigk et al.[55] because there was extensive bile duct proliferation noted. A modified Ishak score[56] was considered and served as a guide to align the animal pathological score with clinical human scoring system.

2.3 *Nonlinear Microscopy*

The nonlinear optical microscope was developed based on a confocal imaging system (LSM 510, Carl Zeiss, Heidelberg, Germany) using an external tunable mode-locked Ti:sapphire laser (Mai-Tai broadband, Spectra-Physics). The system is shown in Fig. 1, where the laser was passed through a pulse compressor (PC), (Femtocontrol, APE GmbH, Berlin, Ger-

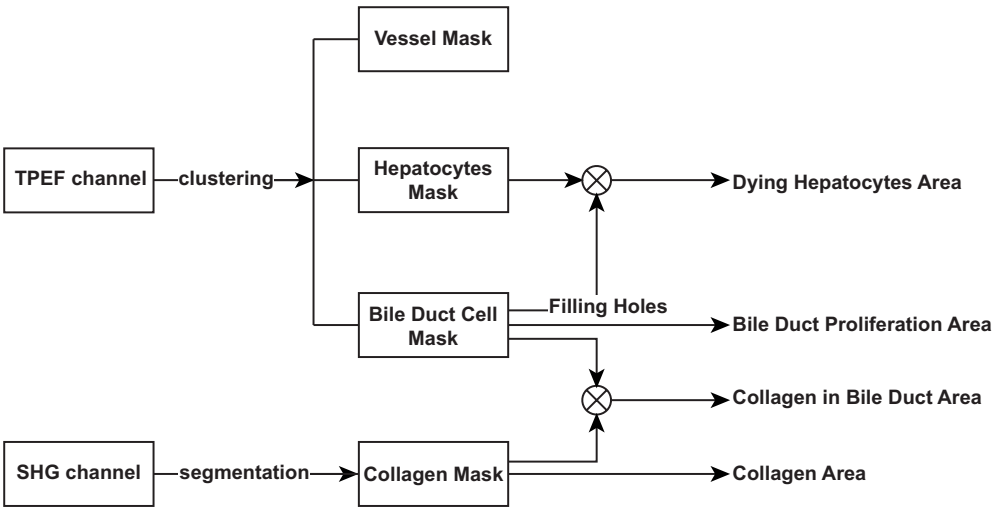

Fig. 2 Flowchart of the feature extraction algorithm. TPEF and SHG two image channels were separated from the same images. The TPEF channel was clustered into three separate masks by intensity difference, namely, bright, dim, and dark. The bright intensity area in the TPEF channel was classified as hepatocytes mask, the dim area was classified as bile duct cell mask and the dark area was classified as vessel mask including outside-tissue space. Collagen mask in the SHG channel was obtained after segmentation was performed on the images. The feature of the total collagen area was then referred to collagen mask and bile duct proliferation area to bile duct cell mask. Multiplying collagen mask and bile duct cell mask yielded the collagen in bile duct area feature. The remnant hepatocytes area feature was defined as clusters of hepatocytes that were surrounded by bile duct cells; therefore, we obtained it by filing holes of the bile duct cell mask, and then multiplying it by hepatocytes mask.

many) and an acousto-optic modulator (AOM) for group velocity dispersion compensation and power attenuation, respectively. The laser was then routed by a dichroic mirror (reflect $>$700 nm, transmit $<$543 nm), through an objective lens [plan-neofluar, 20X, numerical aperture (NA)=0.5, Carl Zeiss, Heidelberg, Germany], to the tissue sample. The average power at the objective lens is ~80 mW. TPEF in the epidirection generated in tissue was collected by the same objective lens and recorded by a photo-multiplier tube (PMT), (Hamamatsu R6357, Tokyo, Japan), after passing through the dichroic mirror (reflect $<$490 nm, transmit $>$490 nm) and a 500–550 nm bandpass (BP) filter. The SHG signal was collected using a condenser (NA=0.55) and filtered by a diaphragm and a 440–460 nm BP filter before entering the PMT for detection. With the intrinsic optical sectioning characteristics for the nonlinear optical process, the pinhole function of the confocal microscope was not used. Reflective SHG signals will be collected along the same optical path as TPEF, but with a different BP filter of 390–465 nm.

2.4 *Image Acquisition and Segmentation*

A total of 12 SHG/TPEF images (3072$\times$3072 pixels, ~1.38$\times$1.38 mm) were scanned for each tissue specimen, with four images covering the liver anterior surface area, four images covering the interior region, and four images covering the posterior surface area. Two specimens were extracted from each animal, with one from the left lobe and one from the right lobe of the liver. For all images, an image-segmentation algorithm based on the mixture Gaussian model was performed to identify collagen areas in SHG channel images. It is assumed that the histogram of intensity of pixels in the image can be modeled as the mixture of two Gaussian distributions, one representing pixels belonging to collagen area with strong SHG signals and the other representing the rest of pixels belonging to noncollagen area. Using the expectation–maximization algorithm,[57] the parameters of the Gaussian distributions was estimated. A binary image was generated by applying a value of 1 to all the pixels having intensity that belongs to the Gaussian distribution representing collagen area and value 0 to the rest of the pixels.

2.5 *Features Extraction and Quantification*

On the liver surface, the tissue edge was detected from the TPEF channel image using the Canny method,[58] which finds edges by looking for local maxima of the gradient in the image. The percentage of collagen of each line, which is parallel to the edge, is calculated. The width of the capsule, which is the unique feature on surface, is defined as the depth where the percentage of collagen changes most between neighboring lines.

Four common features on both the surface (subcapsular region) and in the interior of the liver tissues were quantified, namely, total collagen area percentage, bile duct proliferation area percentage, collagen in bile duct area percentage, and remnant hepatocytes area percentage (Fig. 2). Collagen area percentage is defined as the number of pixels that belongs to collagen in the subcapsular region divided by the total area of the subcapsular region. The segmentation of collagen in the SHG channel image is the same as what is used for capsule identification. Bile duct proliferation area percentage is defined as the number of pixels that belongs to bile duct cells in the subcapsular region divided by the total area of the subcapsular region. Pixels of the TPEF image were clustered into three different groups depending on pixel intensity: completely dark, dim, and bright, which represent areas of the vessel or outside-tissue space, bile duct proliferation area, and hepatocytes, respectively. The clustering was performed by a fuzzy-c-means clustering method.[59,60] In fuzzy clustering, each point has a degree of belonging to clusters rather than belonging completely to just one cluster and associated with

each point is a set of membership levels.[61] These indicate the strength of the association between that data element and a particular cluster. Here we have two clusters, one for collagen and the other for background. $f:\Omega \rightarrow R$ represents SHG image, $x(i,j) \in \Omega$ is the intensity of pixel, and $l \in \Gamma = \{1,2,\ldots,L\}$ is the class label. The objective function to minimize is $J_m = \Sigma_{x \in \Omega l \in \Gamma} \Sigma u_{ij}^m \| f(x) - c_l \|^2$, $1 \leqslant m < \infty$, where u_{ij} is the degree of membership of $x(i,j)$ in cluster l, m is the fuzzyness coefficient, which is a real number of >1. A binary image was generated by applying the value of 1 to all the pixels belonging to the cluster that represents bile duct cell areas and 0 to the rest of the pixels. The collagen in bile duct area percentage is defined as the number of pixels that are collagen and also in bile duct cells area divided by the total area of the subcapsular region. The binary image of collagen in the bile duct area is generated by multiplying the binary images of the collagen area and the bile duct cell area. Remnant hepatocytes are defined as those hepatocytes that are surrounded by bile duct cells. Morphological operations such as erosion, dilation, and hole filling are performed on the binary image of bile duct cell to identify areas surrounded by bile duct cells. If these areas belong to the cluster that represents hepatocytes, then they are recognized as the remnant hepatocytes area. The remnant hepatocytes area percentage is defined as the number of pixels that belongs to the remnant hepatocytes area divided by total area of subcapsular region.

All image-processing and algorithm computations were carried out in MATLAB (The Math Works, Inc., Natick, Massachusetts). The image-processing algorithm code is available for readers on request.

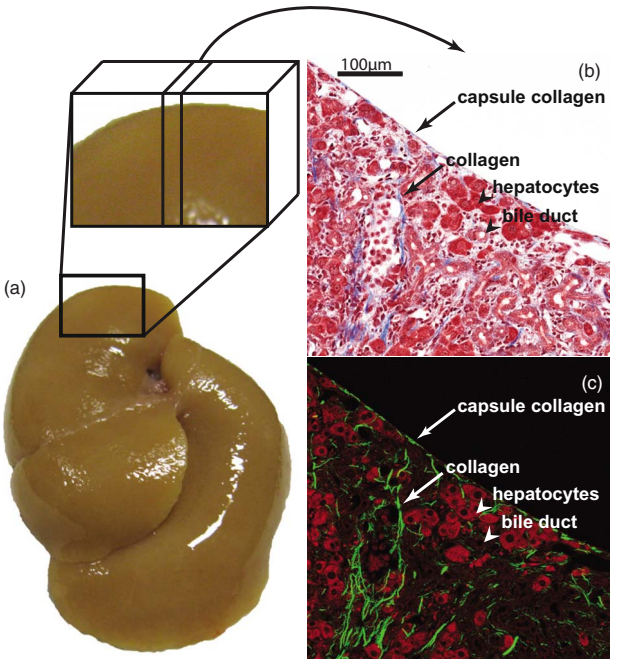

Fig. 3 Comparison between histopathological staining and SHG/TPEF images. (a) A perfused fibrotic tissue was extracted and sectioned perpendicular to its surface to expose the liver boundary [inset in (a)]. (b) MT staining for a fibrotic tissue sample by the direct cutting is shown with collagen stained in blue, cytoplasm in red and cell nuclei in dark brown. (c) The SHG/TPEF image of the same sample is shown with collagen in pseudo green and cells in pseudo red. Features of the capsule collagen, collagen, hepatocytes, and bile duct shown in (b) the staining image can all be identified in (c) the SHG/TPEF image, respectively. Scale bar is 100 μm.

3 Results and Discussions

3.1 *SHG/TPEF Imaging: A Good Substitute for Conventional Histological Imaging*

To explore the surface information in the liver, a perfused liver organ was harvested and tissue samples were extracted to expose the liver surface shown in Fig. 3(a). Liver samples were then sectioned in the direction perpendicular to the surfaces in order to keep the capsular collagen for imaging purposes, as shown in the inset of Fig. 3(a). To validate the use of SHG and TPEF microscopy to quantify morphological changes during fibrosis progression, feature compatibility in both the typical histopathological sections and in SHG/TPEF images was investigated. A histopathological tissue section from a fibrotic liver stained with MT [Fig. 3(b)] is compared to a staining-free SHG/TPEF image [Fig. 3(c)] from the same location with the pseudo-colors of green representing SHG signals and red representing TPEF signals. When compared to the stained image and with the major constituents marked, we observed that both the fibril collagen presented in the internal organ and the capsule collagen in the liver surface can be correctly detected by SHG signals. Because of the presence of intrinsic molecules such as NAD(P)H and flavins, which emit substantial fluorescence after excited with femtopulsed lasers,[62] hepatocytes were easily seen as bright red cells in the SHG/TPEF image [Fig. 3(c)]. Bile duct epithelial cells were shown in Fig. 3(c) as the dim red cells due to their lack of fluorescent molecules. The colocalization of these major features suggests that the pathological development of fibrosis on both the surface and in the interior of liver can be investigated by SHG/TPEF imaging for further quantification.

3.2 *Defining Capsule and Subcapsule Regions on the Liver Surface*

In order to perform a quantitative analysis of liver surface features, we need to define the liver surface with predominantly capsular collagen and the subcapsular region with cells. First, we rotated all images that we obtained into a top empty position whereby there is no tissue sample from the top edge of the image and the liver surface is exposed on the top. Then, combined SHG/TPEF images [Fig. 4(a)] were separated into TPEF [Fig. 4(b)] and SHG [Fig. 4(c)] channels to differentiate the autofluorescence of liver cells from the second harmonic signals of type I collagen. In the TPEF images, the liver boundary was defined as the line boundary between the empty region and the region where there is autofluorescence, and the liver surface is the area below boundary. Because of the morphological difference between the capsule and other liver cells, we separate the surface area into two regions: the capsule and subcapsule regions. The definition of the two was defined in second-harmonic images [Fig. 4(c)]. The SHG image was first converted into a binary image with regions that do not have signals shown as 0 and those with signals as 1. As the line boundary obtained from the red channel was moved pixel by pixel inward, we observed an increase in the average amount of collagen [line average in Fig.

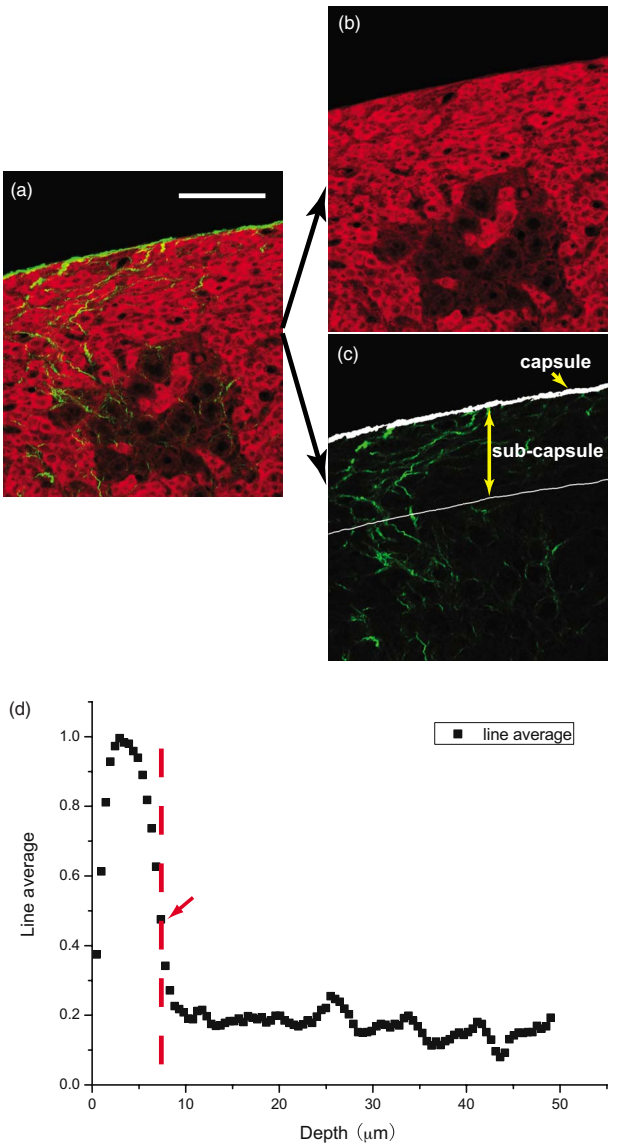

Fig. 4 Definition of capsule and subcapsule regions on the liver surface. The combined (a) SHG/TPEF image was separated into (b) TPEF and (c) SHG channels. After the liver boundary in (b) the TPEF image was identified, collagen content in (c) the SHG image was calculated with the increase in the depth into tissue (d) marked as line average. The depth at which there was a sharp decrease of collagen content [red arrow in (d)] was marked as (c) capsule width, subcapsule region was defined as the region parallel to the tissue. Scale bar is 100 μm.

4(d)] through a maxima and back to its initial value. This defines the thickness of the capsule region. The thick white line in Fig. 4(c) is the capsule region in that image. Tracing parallel to this line, we went deeper into the tissue until we reached a depth where meaningful features or trends could be observed. This defines the thickness of the subcapsule region. We restricted this thickness to 150 μm as the SHG/TPEF signal penetration limit in tissues.

3.3 *Extracting Four Features from Both Surface and Interior Tissue*

With capsule and subcapsule regions defined, we proceed to extract features from the two regions on the surface and in the liver interior. The defined thickness of the capsule region is a unique feature in the surface area. In the subcapsule region of the surface area and in the interior, the parameters included in the study were total collagen, collagen in bile duct areas, bile duct proliferation, and areas occupied by remnant hepatocytes. The feature extraction methods are elaborated in Section 2, and features extracted have been exemplified as binary maps in Fig. 5 based on the same sample image in Fig. 4. Total collagen [Fig. 5(a)] is defined as the percentage of collagen that was presented in SHG images in the sub-capsule and interior area. Bile duct proliferation [Fig. 5(b)] was defined as the percentage of areas in either the subcapsule or the interior that was occupied by bile duct cells. By overlapping Figs. 5(a) and 5(b), we obtained Fig. 5(c), which is the percentage of abnormal collagen that was distributed in the bile duct area. The area occupied by remnant hepatocytes [Fig. 5(d)] is the percentage of areas taken by remnant hepatocytes, defined as small surviving hepatocyte clusters that are surrounded by bile duct cells, in the subcapsule or liver interior. All four features extracted here were based on comparison to the originally stained tissue samples and the pathologist readings.

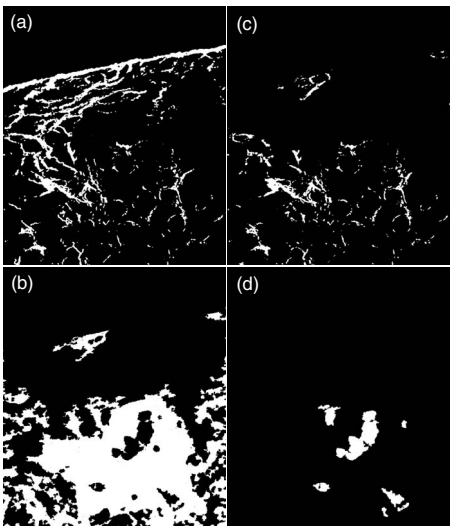

Fig. 5 Feature extraction from SHG/TPEF images. On the basis of the same SHG/TPEF image from Fig. 4, the SHG image was segmented into (a) a binary image representing total collagen in both capsule and subcapsule regions, and liver interior. Bile duct area in the TPEF image was segmented into (b) a bile duct mask. Combining the collagen mask and bile duct mask, (c) the feature of collagen in the bile duct area is shown. (d) Hepatocytes clusters that were surrounded by bile ducts were segmented as remnant hepatocytes.

3.4 *Correlation between Liver Surface and Interior*

To use the features extracted earlier to establish the relationship between the liver surface and interior in fibrosis progression, we first tested the applicability of our features in assessing fibrosis in the liver interior, where most current studies were focused.[48,51] Results [Fig. 6(a)] showed that, with the natural progression of liver fibrosis (weeks 0, 2, 4, and 6 after BDL), total collagen, collagen in bile duct areas, and bile duct proliferation increased significantly across different time points ($p < 0.05$). The dramatic increase of bile duct areas in

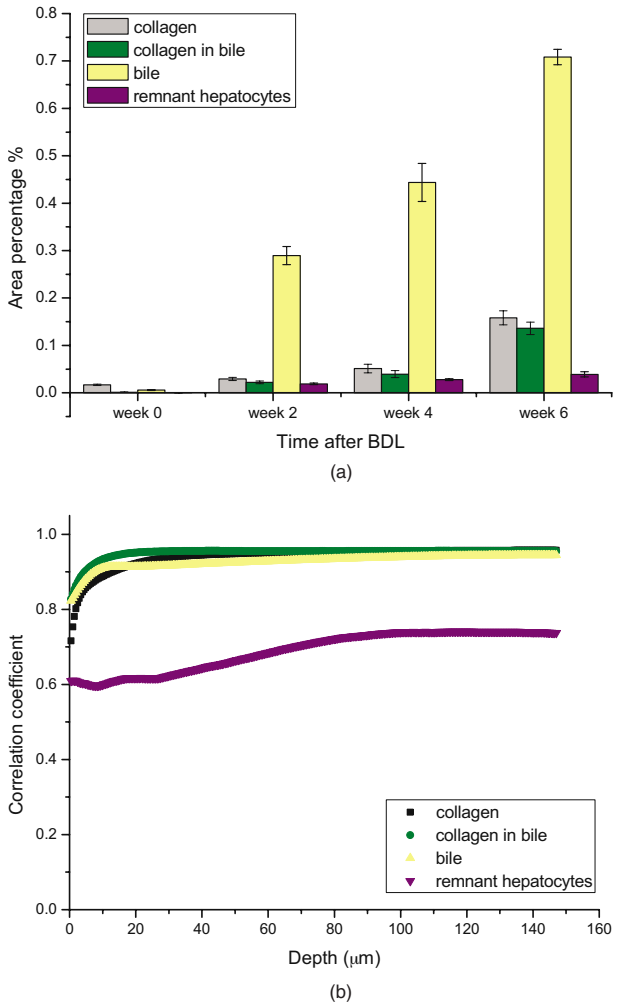

Fig. 6 (a) Comparison of liver surface to interior. In the liver interior, the percentage areas occupied by four different features was shown at different time points after bile duct ligation. All extracted features show a significant ($p<0.05$) upward trend with the fibrosis progression except for remnant hepatocytes between week 4 and week 6. (b) The correlation coefficient of features between the liver interior and surface is shown. Features of total collagen, collagen in bile duct, and bile duct proliferation show an upward trend correlation between surface and interior with the plateau at 20-μm depth in the subcapsule region. Remnant hepatocytes have a lower correlation.

this case is due to the specific model (bile duct ligation) chosen in this study. Comparing the total collagen and collagen in bile duct areas, the levels at each stage are highly similar, indicating a minimal amount of normal collagen in the tissue. The significant difference observed in early stages indicates that collagen in bile is a more sensitive indicator than total collagen to detect fibrosis in liver. Areas occupied by remnant hepatocytes also increased with fibrosis progression; however, no significant difference was detected between weeks 4 and 6 of fibrosis induction, making this feature only a sensible indicator for early stages of fibrosis.

To verify that the four features we extracted are reasonable parameters to quantify liver fibrosis, features were correlated between the liver surface and interior. Because these features were only present in the subcapsule region, the correlation coefficient between the subcapsule region and interior was calculated. Each plot in Fig. 6(b) is the result of comparing the same parameter value obtained from the surface images to the interior images at a particular depth of the subcapsule region. Three of the four parameters studied showed an upward trend in correlation reaching a plateau stage at ~20 μm. The parameter of remnant hepatocytes has a lower correlation, making it a less consistent feature. Therefore, we define our depth of meaningful correlation between the surface and interior regions as 20 μm beneath the liver capsule, beyond which no additional information would be obtained by imaging deeper into the liver tissue.

3.5 *Uniform Fibrosis Distribution across the Anterior Liver Surface*

Studies thus far have been performed on the anterior surface of both the left and right lobes of liver tissue. To understand the relationship between different lobes in order to direct future sampling locations, we calculated the correlation coefficient of two lobes based on the four features at different depths of the subcapsule region. The results [Fig. 7(a)] showed that high feature correlation between the two lobes exists and saturates at 20 μm beneath liver capsule for three quantitative features of total collagen, collagen in bile duct areas, and bile duct proliferation. Thus, we can confidently monitor the progress of fibrosis with either lobe by scanning across their surfaces with no misrepresentation of the extent of fibrosis.

All the quantitative analysis was performed on images from the anterior surface of liver because the scanning of liver surfaces would naturally be performed on the anterior of each lobe. In order to understand the fibrosis progression in a global perspective, we also investigated the correlation between anterior and posterior liver fibrosis. Figure 7(b) showed that lower correlation existed between the anterior and posterior liver surfaces based on pathological features. The correlation between the posterior and interior is also weak (data not shown). This indicated that liver fibrosis progresses in a heterogeneous manner toward anterior and posterior surfaces, with anterior surfaces possessing characteristics similar to the interior. Because the anterior surface is the main focus for surface-scanning purposes, it is less important that there are no highly correlated anterior and posterior surface scans.

3.6 *Features on or near the Liver Surface are a Good Indication of Liver Fibrosis*

Because the liver surface is highly correlated with the interior with the morphological features stated above and the fibrosis distribution is relatively uniform across the liver anterior surface, we focused on the anterior liver surface to quantitatively assess liver fibrosis. A sub-capsule region of 20 μm was shown as an example here because it represents the minimal sampling amount for the meaningful correlation of surface and interior. With a 50-μm thickness of the tissue slices and scanning length of 1380 μm on the anterior surface, an area of 69,000 μm^2 on the liver surface was covered by each SHG/TPEF image, which is smaller than the equivalent surface area of 225,625 μm^2, a nonlinear endomicroscopy can scan.[53] The same four features [Fig. 8(a)] were extracted in the subcapsule region, with each quantified at different time points (week 0, 2, 4, and 6 after BDL). Conventional assess-

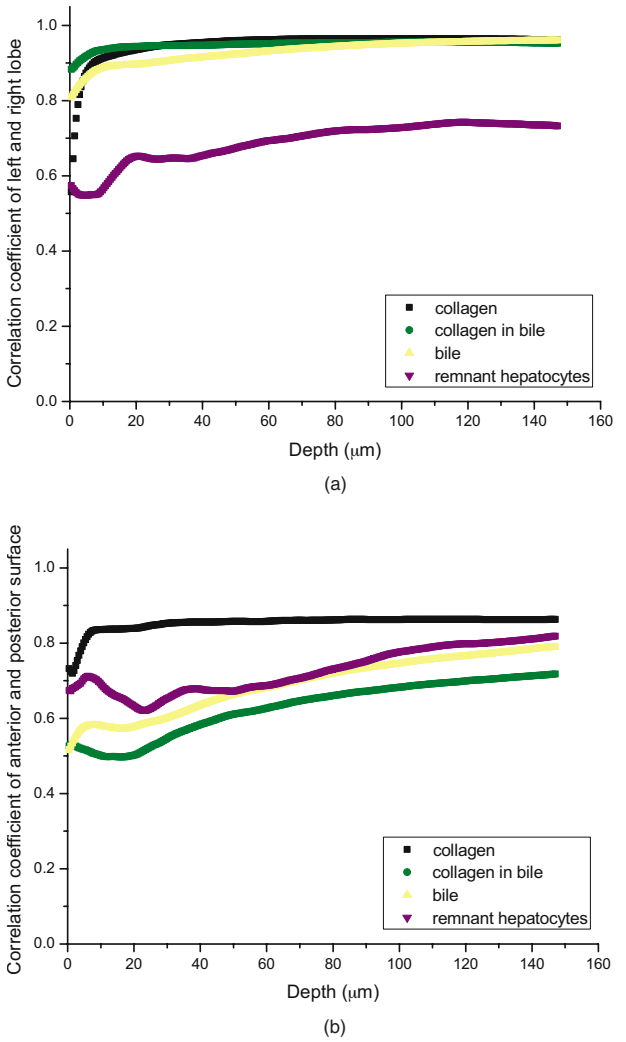

Fig. 7 Quantification of the fibrosis distribution on the liver surface. (a) The correlation coefficients of the left and right liver lobe surface features are shown. Except for the feature of remnant hepatocytes that are less correlated, all other surface features have high correlations reaching a plateau at the subcapsule depth of 20 μm. (b) The correlation coefficient of the anterior and posterior surface features remains at low level, indicating less correlation between these two surfaces.

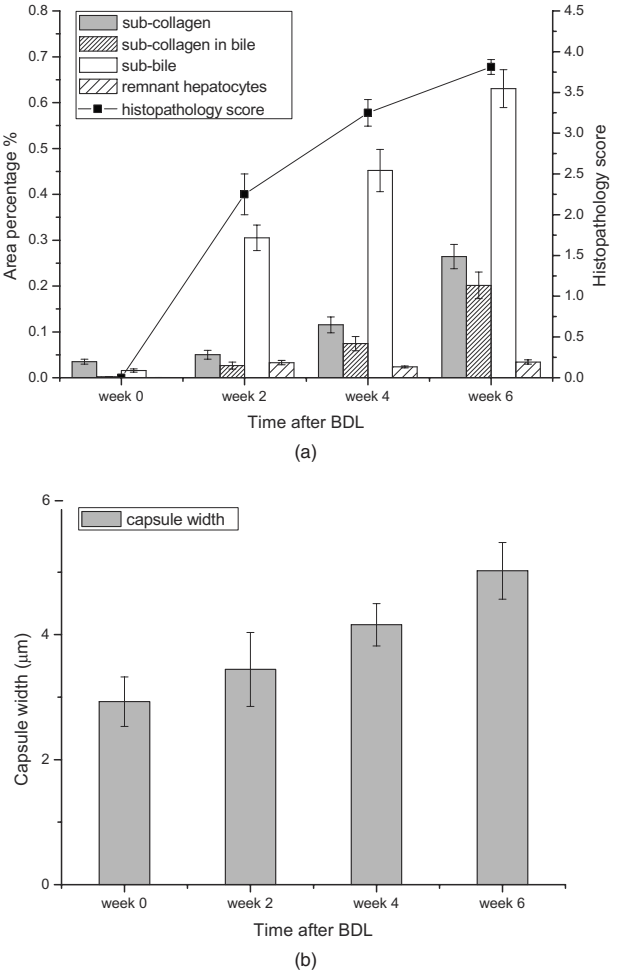

Fig. 8 Quantification of liver fibrosis progression on the liver surface. (a) Quantification results of different features extracted from SHG/TPEF images obtained at different time points after BDL showed an upward trend with the fibrosis progression in all features. Significant differences among different time points exist for collagen in the bile duct area and bile duct proliferation in the subcapsule region. This upward trend also agrees with the histopathology scoring results of the same stained tissue samples. (b) Capsule width in the capsule region also increases with the fibrosis progression, with more significant increases in the late stage of fibrosis.

ment based on the histopathological scoring system[54] was also performed in all tissue samples as control. Fibrosis was scored in five stages, 0, 1, 2, 3, 4, with stage 0 denoting no fibrosis and stage 4 denoting the most advanced fibrosis or cirrhosis. In the subcapsule region [Fig. 8(a)], features of total collagen, collagen in bile duct areas, and bile duct proliferation have close agreement with the histopathological scores. The differences between different time points are also significant ($P < 0.05$) except for total collagen in early stages (between weeks 0 and 2). Areas occupied by remnant hepatocytes, as a less-correlated feature between surface and interior, did not show an observable trend with the progression of fibrosis on the surface; however, just as in the interior, remnant hepatocytes on the liver surface can be a good indicator for the occurrence of fibrosis.

Buschmann and Ryoo[63] suggested that capsular collagen width could be used as a measurement of fibrosis, along with the capsule thickening in liver disease. Here, we quantified the capsule collagen width based on our capsule definition [Fig. 8(b)] as a unique feature in the surface area. The trend of increasing thickness with fibrogenesis in our model confirmed the nonquantitative findings in the previous study.[63,64] However, we cannot make a clear distinction between each consecutive stage based on statistically significant analysis of this feature even though we can differentiate between the early and late stages of BDL. Therefore, quantification of liver fibrosis on the liver surface works well when SHG and TPEF microscopy enables the quantitative imaging of liver tissue beneath the collagen capsule.

3.7 *Application in Liver Surface Scanning*

With the anterior liver surface containing the similar features as in the liver interior, we compared the normal and fibrotic anterior liver surface by scanning on the front size of the

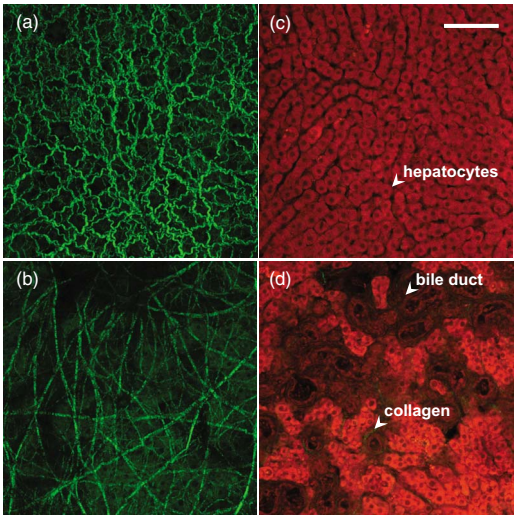

Fig. 9 Liver anterior surface scanning. Front size images from liver surfaces were obtained by reflective SHG and TPEF imaging. 3-D projections of capsule regions were shown in both (a) normal and (c) fibrotic liver. Irregular and less aligned capsule collagen distribution in fibrotic liver is observed compared to normal liver with denser collagen fibers or bundles with curry subfilament structures. Subcapsule region images were obtained 20 μm beneath the capsule region in (b) normal and (d) fibrotic liver tissues. Features of bile duct and abnormal collagen proliferations were present in (d) fibrotic liver compared to (b) normal liver, where only well-organized hepatocytes were present. Scale bar is 100 μm.

perfused liver using reflective mode SHG and TPEF (Fig. 9). In the capsule region in normal liver [Fig. 9(a)], capsule collagen fibers or fibrous bundles are dense with curry subfilament structures [Fig. 9(c)]. In fibrotic liver, the capsular collagen fibers or fibrous bundles are less dense and straight with loss of curry subfilament structures, likely due to the expansion force in liver (portal hypertension and venopathy, which cause an increase in liver stiffness and cirrhosis[65].) And 20 μm beneath the capsule region in the subcapsule region, normal liver [Fig. 9(b)] has well-organized hepatocytes and no clear collagen presence. While in the BDL fibrotic liver [Fig. 9(d)], bile duct proliferation is obvious that destroys some functional hepatocytes. Abnormal collagen is also present around the bile duct cells, which is a clear indication of fibrosis. Most features are consistent in both the reflective- and transmission-mode images, although the SHG and TPEF signals are weaker in the reflective-mode images. Significant signals can be collected up to 30 μm for SHG and 40 μm for TPEF signals beneath the capsular surface, which is deeper than the statistically meaningful depth of 20 μm to differentiate the normal and fibrotic livers.

4 Conclusions

We discovered a strong correlation between liver fibrosis progression on the anterior surface and the liver interior based on quantitative analysis of morphological features in both regions. Using SHG and TPEF microscopy, we demonstrated the feasibility of monitoring liver fibrosis progression on the anterior surface with the BDL animal model by comparing to the conventional histopathological scoring system. We also discovered a uniform distribution of quantitative liver fibrotic features, such as total collagen distribution, bile duct proliferation, and collagen in bile duct areas, across two main lobes of the anterior liver surface, which gave us confidence to quantitatively monitor the progress of liver fibrosis on different lobe surfaces. We are now one step closer to applying reflective or laparoscopic imaging of the liver surface to stage liver fibrosis, which can potentially be used clinically to complement or eventually replace the more invasive liver biopsy.

Acknowledgments

We thank members of the Cell and Tissue Engineering Laboratory for technical support and scientific discussion. This work is supported in part by the intramural funding from the Institute of Bioengineering and Nanotechnology, BMRC, A*STAR of Singapore and Grants No. R-185-000-182-592 (Janssen Cilag) and Singapore-MIT Alliance Computational and Systems Biology Flagship Project (Grant No. C-382-641-001-091), SMART, and Mechanobiology Institute, Singapore (Grant No. R-714-001-003-271) funding to H.Y.

References

1. S. L. Friedman, "Seminars in medicine of the Beth Israel Hospital, Boston. The cellular basis of hepatic fibrosis. Mechanisms and treatment strategies," *New Engl. J. Med.* **328**(25), 1828–1835 (1993).
2. S. L. Friedman, "Molecular regulation of hepatic fibrosis, an integrated cellular response to tissue injury," *J. Biol. Chem.* **275**(4), 2247–2250 (2000).
3. S. L. Friedman, "Liver fibrosis—from bench to bedside," *J. Hepatol* **38**(Suppl 1), S38–53 (2003).
4. J. B. Dixon, P. S. Bhathal, N. R. Hughes, and P. E. O'Brien, "Nonalcoholic fatty liver disease: improvement in liver histological analysis with weight loss," *Hepatology (Philadelphia, PA, U. S.)* **39**(6), 1647–1654 (2004).
5. P. Farci et al., "Long-term benefit of interferon alpha therapy of chronic hepatitis D: regression of advanced hepatic fibrosis," *Gastroenterology* **126**(7), 1740–1749 (2004).
6. A. J. Fowell and J. P. Iredale, "Emerging therapies for liver fibrosis," *Dig. Dis.* **24**(1–2), 174–183 (2006).
7. S. L. Friedman and M. B. Bansal, "Reversal of hepatic fibrosis—fact or fantasy?" *Hepatology (Philadelphia, PA, U. S.)* **43**(2 Suppl 1), S82–88 (2006).
8. M. J. Arthur, "Reversibility of liver fibrosis and cirrhosis following treatment for hepatitis C," *Gastroenterology* **122**(5), 1525–1528 (2002).
9. Z. D. Goodman, "Grading and staging systems for inflammation and fibrosis in chronic liver diseases," *J. Hepatol* **47**(4), 598–607 (2007).
10. N. Assy and G. Y. Minuk, "Serum aspartate but not alanine aminotransferase levels help to predict the histological features of chronic hepatitis C viral infections in adults," *Am. J. Gastroenterol.* **95**(6), 1545–1550 (2000).
11. F. H. Anderson, L. Zeng, N. R. Rock, and E. M. Yoshida, "An assessment of the clinical utility of serum ALT and AST in chronic hepatitis C," *Hepatol Res.* **18**(1), 63–71 (2000).
12. C. T. Wai, J. K. Greenson, R. J. Fontana, J. D. Kalbfleisch, J. A. Marrero, H. S. Conjeevaram, and A. S. Lok, "A simple noninvasive index can predict both significant fibrosis and cirrhosis in patients with chronic hepatitis C," *Hepatology (Philadelphia, PA, U. S.)* **38**(2), 518–526 (2003).
13. N. V. Chrysanthos, G. V. Papatheodoridis, S. Savvas, G. Kafiri, K. Petraki, E. K. Manesis, and A. J. Archimandritis, "Aspartate aminotransferase to platelet ratio index for fibrosis evaluation in chronic viral hepatitis," *Eur. J. Gastroenterol. Hepatol* **18**(4), 389–396 (2006).
14. A. A. Shaheen and R. P. Myers, "Diagnostic accuracy of the aspartate aminotransferase-to-platelet ratio index for the prediction of hepatitis C-related fibrosis: a systematic review," *Hepatology (Philadelphia, PA, U. S.)* **46**(3), 912–921 (2007).
15. K. M. Walsh, A. Fletcher, R. N. MacSween, and A. J. Morris, "Basement membrane peptides as markers of liver disease in chronic hepa-

titis C," *J. Hepatol* **32**(2), 325–330 (2000).
16. S. Kanzler, M. Baumann, P. Schirmacher, V. Dries, E. Bayer, G. Gerken, H. P. Dienes, and A. W. Lohse, "Prediction of progressive liver fibrosis in hepatitis C infection by serum and tissue levels of transforming growth factor-beta," *J. Viral Hepat.* **8**(6), 430–437 (2001).
17. D. K. George, G. A. Ramm, N. I. Walker, L. W. Powell, and D. H. Crawford, "Elevated serum type IV collagen: a sensitive indicator of the presence of cirrhosis in haemochromatosis," *J. Hepatol* **31**(1), 47–52 (1999).
18. P. Fabris et al., "Fibrogenesis serum markers in patients with chronic hepatitis C treated with alpha-IFN," *J. Gastroenterol.* **34**(3), 345–350 (1999).
19. M. Larrousse et al., "Noninvasive diagnosis of hepatic fibrosis in HIV/HCV-coinfected patients," *J. Acquired Immune Defic. Syndr.* **46**(3), 304–311 (2007).
20. J. G. McHutchison, L. M. Blatt, M. de Medina, J. R. Craig, A. Conrad, E. R. Schiff, and M. J. Tong, "Measurement of serum hyaluronic acid in patients with chronic hepatitis C and its relationship to liver histology. Consensus Interferon Study Group," *J. Gastroenterol. Hepatol* **15**(8), 945–951 (2000).
21. J. C. Trinchet, "Clinical use of serum markers of fibrosis in chronic hepatitis," *J. Hepatol* **22**(2 Suppl), 89–95 (1995).
22. D. Thabut, M. Simon, R. P. Myers, D. Messous, V. Thibault, F. Imbert-Bismut, and T. Poynard, "Noninvasive prediction of fibrosis in patients with chronic hepatitis C," *Hepatology (Philadelphia, PA, U. S.)* **37**(5), 1220–1221; author reply, 1221 (2003).
23. D. S. Manning and N. H. Afdhal, "Diagnosis and quantitation of fibrosis," *Gastroenterology* **134**(6), 1670–1681 (2008).
24. C. Aube et al., "Ultrasonographic diagnosis of hepatic fibrosis or cirrhosis," *J. Hepatol* **30**(3), 472–478 (1999).
25. M. Fraquelli, C. Rigamonti, G. Casazza, D. Conte, M. F. Donato, G. Ronchi, and M. Colombo, "Reproducibility of transient elastography in the evaluation of liver fibrosis in patients with chronic liver disease," *Gut* **56**(7), 968–973 (2007).
26. N. Salameh, F. Peeters, R. Sinkus, J. Abarca-Quinones, L. Annet, L. C. Ter Beek, I. Leclercq, and B. E. Van Beers, "Hepatic viscoelastic parameters measured with MR elastography: correlations with quantitative analysis of liver fibrosis in the rat," *J. Magn. Reson Imaging* **26**(4), 956–962 (2007).
27. M. Yin, J. A. Talwalkar, K. J. Glaser, A. Manduca, R. C. Grimm, P. J. Rossman, J. L. Fidler, and R. L. Ehman, "Assessment of hepatic fibrosis with magnetic resonance elastography," *Clin. Gastroenterol.* **5**(10), 1207–1213 (2007).
28. J. Perrault, D. B. McGill, B. J. Ott, and W. F. Taylor, "Liver biopsy: complications in 1000 inpatients and outpatients," *Gastroenterology* **74**(1), 103–106 (1978).
29. N. J. Torok, "Recent advances in the pathogenesis and diagnosis of liver fibrosis," *J. Gastroenterol.* **43**(5), 315–321 (2008).
30. J. Poniachik, D. E. Bernstein, K. R. Reddy, L. J. Jeffers, M. E. CoelhoLittle, F. Civantos, and E. R. Schiff, "The role of laparoscopy in the diagnosis of cirrhosis," *Gastrointest. Endosc.* **43**(6), 568–571 (1996).
31. L. Pagliaro et al., "Percutaneous blind biopsy versus laparoscopy with guided biopsy in diagnosis of cirrhosis. a prospective, randomized trial," *Dig. Dis. Sci.* **28**(1), 39–43 (1983).
32. B. Maharaj, R. J. Maharaj, W. P. Leary, R. M. Cooppan, A. D. Naran, D. Pirie, and D. J. Pudifin, "Sampling variability and its influence on the diagnostic yield of percutaneous needle biopsy of the liver," *Lancet* **1**(8480), 523–525 (1986).
33. R. Jalan, D.F. Harrison , J. F.Dillon , R. A.Elton ,N. D. C. Finlayson , and P. C. Hayes ,"Laparoscopy and histology in the diagnosis of chronic liver-disease," *QJM* **88**(8), 559–564 (1995).
34. J. Poniachik D. E. Bernstein, K. R. Reddy, L. J. Jeffers, M. E. CoelhoLittle, F. Civantos, and E. R. Schiff, "The role of laparoscopy in the diagnosis of cirrhosis," *Gastrointest. Endosc.* **43**(6), 568–571 (1996).
35. X. Han, Ryan M. Burke, Martha L. Zettel, Ping Tang, and Edward B. Brown, "Second harmonic properties of tumor collagen: determining the structural relationship between reactive stroma and healthy stroma," *Opt. Express* **16**(3), 1846–1859 (2008).
36. T. A. Theodossiou, C. Thrasiovoulou, C. Ekowobi, and D. L. Becker, "Second harmonic generation confocal microscopy of collagen type I from rat tendon cryosections," *Biophys. J.* **91**(12), 4665–4677 (2006).
37. B. A. Nemet, V. Nikolenko, and R. Yuste, "Second harmonic imaging of membrane potential of neurons with retinal," *J. Biomed. Opt.* **9**(5), 873–881 (2004).
38. Sung-Jan Lin, Ruei Wu Jr., Hsin-Yuan Tan, Wen Lo, Wei-Chou Lin, Tai-Horng Young, Chih-Jung Hsu, Jau-Shiuh Chen, Shiou-Hwa-Jee, and Chen-Yuan Dong,, "Evaluating cutaneous photoaging by use of multiphoton fluorescence and second-harmonic generation microscopy," *Opt. Lett.* **30**(17), 2275–2277 (2005).
39. V. Nucciotti, C. Stringari, L. Sacconi, F. Vanzi, L. Fusi, M. Linari, G. Piazzesi, V. Lombardi, and F. S. Pavone,"Probing myosin structural conformation in vivo by second-harmonic generation microscopy," *Proc. Natl. Acad. Sci. U.S.A.* **107**(17), 7763–7768 (2010).
40. P. J. Campagnola, A. C. Millard, M. Terasaki, P. E. Hoppe, C. J. Malone, and W. A. Mohler, "Three-dimensional high-resolution second-harmonic generation imaging of endogenous structural proteins in biological tissues," *Biophys. J.* **82**(1 Pt 1), 493–508 (2002).
41. S. W. Teng et al., "Multiphoton fluorescence and second-harmonic-generation microscopy for imaging structural alterations in corneal scar tissue in penetrating full-thickness wound," *Arch. Ophthalmol. (Chicago)* **125**(7), 977–978 (2007).
42. B. Gong, J. Sun, G. Vargas, Q. Chang, Y. Xu, D. Srivastava, and P. J. Boor, "Nonlinear imaging study of extracellular matrix in chemical-induced, developmental dissecting aortic aneurysm: evidence for defective collagen type III," *Birth Defects Res A* **82**(1), 16–24 (2008).
43. E. J. Gualda, G. Filippidis, G. Voglis, M. Mari, C. Fotakis, and N. Tavernarakis, "*In vivo* imaging of cellular structures in Caenorhabditis elegans by combined TPEF, SHG and THG microscopy," *J. Microsc.* **229**(Pt 1), 141–150 (2008).
44. J. G. Lyubovitsky, T. B. Krasieva, X. Xu, B. Andersen, and B. J. Tromberg, "*In situ* multiphoton optical tomography of hair follicles in mice," *J. Biomed. Opt.* **12**(4), 044003 (2007).
45. T. Z. Teisseyre, A. C. Millard, P. Yan, J. P. Wuskell, A. Lewis, and L. M. Loew, "Nonlinear optical potentiometric dyes optimized for imaging with 1064-nm light," *J. Biomed. Opt.* **12**(4), 044001 (2007).
46. M. Strupler, "Second harmonic imaging and scoring of collagen in fibrotic tissues," *Opt. Express* **15**(7), 4054–4065 (2007).
47. C. Odin, Y. Le Grand, A. Renault, L. Gailhouste, and G. Baffet, "Orientation fields of nonlinear biological fibrils by second harmonic generation microscopy," *J. Microsc.* **229**(Pt 1), 32–38 (2008).
48. W. Sun, S. Chang, D. C. Tai, N. Tan, G. Xiao, H. Tang, and H. Yu, "Nonlinear optical microscopy: use of second harmonic generation and two-photon microscopy for automated quantitative liver fibrosis studies," *J. Biomed. Opt.* **13**(6), 064010 (2008).
49. M. D. Gorrell, X. M. Wang, M. T. Levy, E. Kable, G. Marinos, G. Cox, and G. W. McCaughan, "Intrahepatic expression of collagen and fibroblast activation protein (FAP) in hepatitis C virus infection," *Adv. Exp. Med. Biol.* **524**, 235–243 (2003).
50. G. Cox, E. Kablle, A. Jones, I. Fraser, F. Manconi, and M. D. Gorrell, "3-dimensional imaging of collagen using second harmonic generation," *J. Struct. Biol.* **141**(1), 53–62 (2003).
51. D. C. Tai et al., "Fibro-C-Index: comprehensive, morphology-based quantification of liver fibrosis using second harmonic generation and two-photon microscopy," *J. Biomed. Opt.* **14**(4), 044013 (2009).
52. Y. Wu, Y. Leng, J. Xi, and X. Li, "Scanning all-fiber-optic endomicroscopy system for 3D nonlinear optical imaging of biological tissues," *Opt. Express* **17**(10), 7907–7915 (2009).
53. H. Bao, A. Boussioutas, R. Jeremy, S. Russell, and M. Gu, "Second harmonic generation imaging via nonlinear endomicroscopy," *Opt. Express* **18**(2), 1255–1260 (2009).
54. M. J. Ruwart et al., "The integrated value of serum procollagen III peptide over time predicts hepatic hydroxyproline content and stainable collagen in a model of dietary cirrhosis in the rat," *Hepatology (Philadelphia, PA, U. S.)* **10**(5), 801–806 (1989).
55. G. Boigk, L. Stroedter, H. Herbst, J. Waldschmidt, E. O. Riecken, and D. Schuppan, "Silymarin retards collagen accumulation in early and advanced biliary fibrosis secondary to complete bile duct obliteration in rats," *Hepatology (Philadelphia, PA, U. S.)* **26**(3), 643–649 (1997).
56. K. Ishak et al., "Histological grading and staging of chronic hepatitis," *J. Hepatol* **22**(6), 696–629 (1995).
57. A. P. Dempster, N. M. Laird, and D. B. Rubin, "Maximum likelihood from incomplete data via em algorithm," *J. R. Stat. Soc. Ser. B (Methodol.)* **39**(1), 1–38 (1977).
58. J. Canny, "A Computational approach to edge-detection," *IEEE Trans. Pattern Anal. Mach. Intell.* **8**(6), 679–698 (1986).
59. P. H. Wang, "Pattern-recognition with fuzzy objective function

algorithms—bezdek, JC.," *SIAM Rev.* **25**(3), 442–442 (1983).
60. N. Zahid, O. Abouelala, M. Limouri, and A. Essaid, "Fuzzy clustering based on K-nearest-neighbours rule," *Fuzzy Sets Syst.* **120**(2), 239–247 (2001).
61. J. C. Bezdek, *Pattern Recognition with Fuzzy Objective Function Algorithms*, Kluwer Academic Publishers (1981).
62. W. R. Zipfel, R. M. Williams, R. Christie, A. Y. Nikitin, B. T. Hyman, and W. W. Webb, "Live tissue intrinsic emission microscopy using multiphoton-excited native fluorescence and second harmonic generation," *Proc. Natl. Acad. Sci. U.S.A.* **100**(12), 7075–7080 (2003).
63. R. J. Buschmann and J. W. Ryoo, "Hepatic structural correlates of liver fibrosis: a morphometric analysis," *Exp. Mol. Pathol.* **50**(1), 114–124 (1989).
64. J. W. Ryoo and R. J. Buschmann, "Comparison of intralobar nonparenchyma, subcapsular non-parenchyma, and liver capsule thickness," *J. Clin. Pathol.* **42**(7), 740–744 (1989).
65. L. Castera, J. Vergniol, J. Foucher, B. Le Bail, E. Chanteloup, M. Haaser, M. Darriet, P. Couzigou, and V. De Ledinghen, "Prospective comparison of transient elastography, Fibrotest, APRI, and liver biopsy for the assessment of fibrosis in chronic hepatitis C," *Gastroenterology* **128**(2), 343–350 (2005).